Sensors and Materials, Vol. 35, No. 12 (2023) 4359–4381
MYU Tokyo

S & M 3486

Adaptable Algorithm for Tracking Global Maximum Power Point of Photovoltaic Module Arrays

Kuei-Hsiang Chao,* Ying-Piao Kuo, and Hong-Han Chen

Department of Electrical Engineering, National Chin-Yi University of Technology,
No. 57, Sec. 2, Zhongshan Rd., Taiping Dist., Taichung 41170, Taiwan

(Received May 11, 2023; accepted December 5, 2023)

Keywords: grey wolf optimization algorithm, photovoltaic module array, global maximum power point tracking, partial shading, high step-up, soft-switching converter, multiple peak values of power–voltage characteristic curve

The main objective of this study was to develop a method for the maximum power point tracking (MPPT) of photovoltaic module arrays (PVMAs) implemented using two proposed improved grey wolf optimization algorithms (GWOAs). A high-step-up soft-switching converter combined with lost-cost voltage and current sensors was adopted to realize MPPT. This reduced the converter switching losses and cost. Furthermore, in the improved GWOAs, iteration parameters were automatically adjusted online on the basis of the slope of the power–voltage (*P–V*) curve of the PVMA. In addition, 0.8 times the maximum power point (MPP) voltage of the PVMAs under standard test conditions was set as the starting voltage for conducting global MPPT. Lastly, by verifying the proposed improved GWOAs with actual test results, where multiple peak values were generated in the *P–V* characteristic curve of the PVMA by shading, we demonstrated that all MPPs could be tracked successfully, and the two improved GWOAs reduced the tracking time by at least 18.6 and 33.3% compared with that of the conventional GWOA. Therefore, the improved GWOAs exhibit superior tracking speed and stability.

1. Introduction

In a photovoltaic module array (PVMA), solar radiance and temperature fluctuations cause output *P–V* characteristic curves to exhibit nonlinear changes. Therefore, maximum power point tracking (MPPT) technology is necessary to ensure that the PVMA is capable of tracking the maximum power point (MPP) in a changing environment. Currently, conventional perturbation and observation (P&O) is a commonly used method for MPPT,[1,2] where perturbation is achieved by increasing the fixed duty cycle or reducing the voltage. If the voltage perturbation leads to an increase (decrease) in power output, the next perturbation is executed in the same (opposite) direction. Although the P&O method has advantages such as a simple architecture and measurement parameters, it fails to precisely track the true MPP, and oscillations occur near the MPP. When changes in solar radiance are large, timely adjustments cannot be made, and

*Corresponding author: e-mail: chaokh@ncut.edu.tw
https://doi.org/10.18494/SAM4645

ISSN 0914-4935
https://myukk.org/

adjustments can easily be affected by power surges, which cause operational failure. Furthermore, although the application of the P&O method with the *P–V* characteristic curve of the PVMA having a single peak value leads to the successful tracking of the MPP, the *P–V* characteristic curve will generate multiple peaks if the malfunction or shading of the photovoltaic module occurs. Although this may be detected by the local maximum power point (LMPP) during tracking, the tracking of a globally true MPP will not be possible.

Several smart MPPT methods have been proposed for the control of multiple peak values caused by the shading of some modules in a PVMA that generate characteristic *P–V* curves.[3–15] One of these MPPT methods is ant colony optimization (ACO).[5] This algorithm has few setting parameters and a simple structure, but its search speed is low, reducing its suitability for finding an optimal path quickly. Although artificial bee colony optimization also requires few setting parameters and is fast,[6,7] its tracking speed, convergence, and stability are affected by the number of scouting bees, and this may result in an excessively long tracking response time. On the other hand, particle swarm optimization (PSO), based on a study of bird feeding behavior,[8,9] requires relatively few iterations of swarm evolution compared with other similar algorithms. However, a problem can arise when this algorithm becomes trapped in a local solution and fails to achieve precise search results. Although the genetic algorithm (GA) has outstanding optimum search characteristics, which allow the system to converge slowly,[10,11] when it is applied independently, longer calculation times might be needed for large swarms, which also leads to longer tracking times. Teaching–learning-based optimization (TLBO) is a swarm intelligence optimization algorithm proposed by Rao *et al.* in 2011,[12,13] which was inspired by the interaction between a teacher and students. TLBO has swarm memory characteristics and scatter searching similar to those of ACO and PSO, where the principle is easy to comprehend and few setting parameters are required. However, student levels differ and the teaching–learning factor range is smaller. The implementation of inadequate teaching–learning parameters may result in poor learning efficiency and excessively long response and tracking times. The cuckoo search algorithm (CSA) is also a swarm intelligence optimization algorithm and was proposed by Ahmed and Salam[14] and Soneji and Sanghvi.[15] However, fixed steps are used in the conventional CSA for the upper and lower search range limits, and searching continues until the global maximum power point (GMPP) is located. GMPP tracking takes a long time and can be impeded by back-and-forth oscillation between temporary and steady states. A combination of an intelligent algorithm with the conventional MPPT has also been proposed,[16,17] where it was suggested that PSO or GA be integrated with the P&O method. However, although the combined method was capable of finding the global optimum, the response time and tracking speed were still unsatisfactory.

Therefore, because of the shortcomings mentioned above, we proposed two improved GWOAs in this study, which allows the *P–V* characteristics of a PVMA to be quickly tracked.[18–20] GMPP tracking was found to be fast and successful even in the presence of multiple peaks caused by the partial shading or malfunction of some photovoltaic modules. These approaches provided good tracking speed as well as excellent steady-state performance. It can also reduce the cost and improve the efficiency of tracking. In addition, a high-step-up soft-switching converter previously developed by the authors combined with simple voltage and current sensors was used for the MPPT of a PVMA.[21]

2. Characteristics of PVMA

The PVMA in a photovoltaic power generation system consists of several modules connected in series and parallel. Many different and changing environmental conditions, such as tall trees, buildings, clouds, dust, and dirt, will cause the shading of the PVMA, reducing the output power from the array and generating multiple peaks in the output *P–V* characteristic curve. To explore the characteristics of a PVMA under intermittent shading conditions, a SunWorld SWM-20W unit with four modules in series and three in parallel[22] was used for the experiments in this study. In Table 1, the electrical parameter specifications for a single SWM-20W photovoltaic module are displayed.[22] Figure 1 shows a MATLAB simulation of a PVMA with four modules in series and three in parallel under standard test conditions (STCs), where the output *I–V* and *P–V* characteristic curves for a different shading ratio on each module in two different series are displayed. From Fig. 1, it can be seen that when the modules in different series have different shading ratios, the *P–V* characteristic curve has multiple peaks. Figure 2 displays the architecture of an improved MPPT controller based on the improved GWOA proposed in this paper.

Table 1
Electrical parameter specifications for SWM-20W photovoltaic module.[22]

Parameter	Value
Maximum output power, P_{max}	20 W
Current of maximum output power point, I_{mpp}	1.10 A
Voltage of maximum output power point, V_{mpp}	18.18 V
Short-circuit current, I_{sc}	1.15 A
Open-circuit voltage, P_{maxoc}	22.32 V

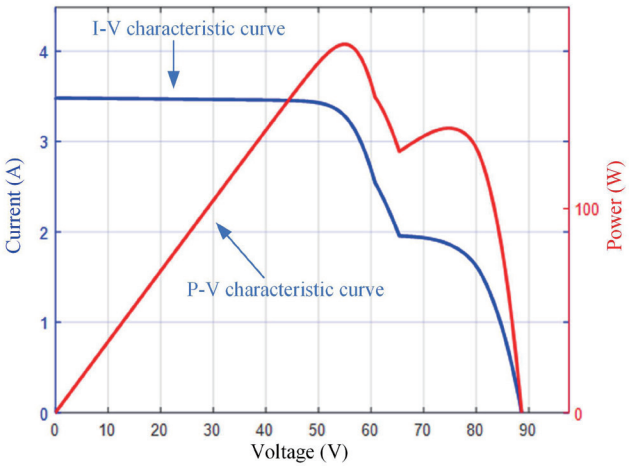

Fig. 1. (Color online) Output *I–V* and *P–V* characteristic curves for a PVMA (model SWM-20W) under STCs, where each module in the two different series has a different shading ratio.

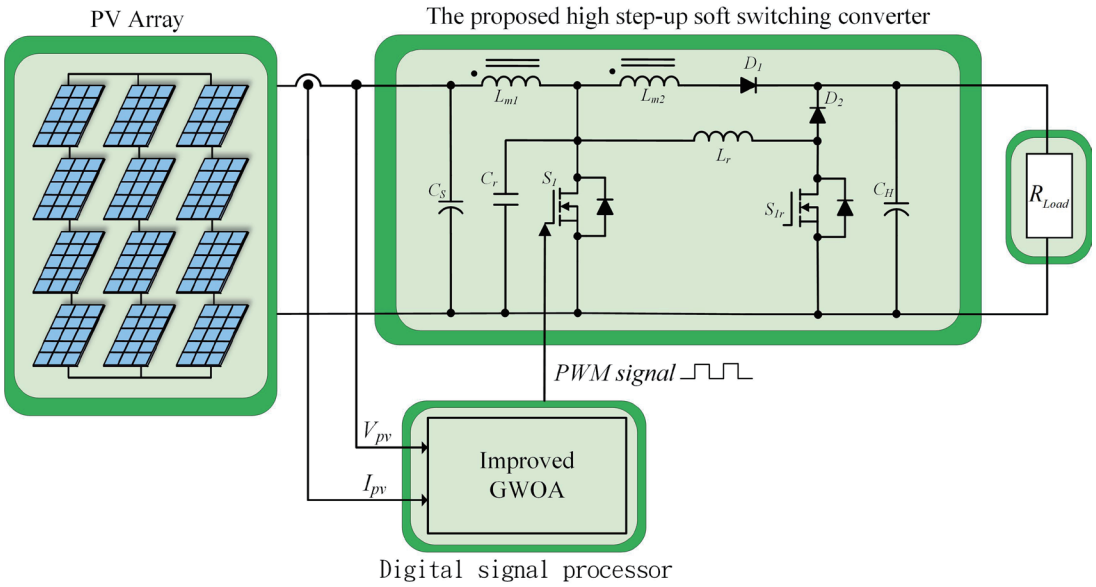

Fig. 2. (Color online) Architecture of the MPPT controller based on the improved GWOA.

3. Grey Wolf Optimization Algorithm

The GWOA is a swarm intelligence optimization algorithm proposed by Mirjalili *et al.* in 2014,[18] which mimics the social hierarchy and hunting mechanism of grey wolves in nature.[18–20] The hunting mechanism has three stages, namely, surround, pursue, and attack, where hunting is carried out by wolves at different levels in the social hierarchy. The continuous renewal of grey wolves at the highest level in the hierarchy eventually leads to a globally optimized search.

In this algorithm, the positions of the highest ranked grey wolves are continually updated in the search for global optimal values. The GWOA includes the following advantages. (a) Easy to realize: The implementation of this algorithm is relatively simple. It only requires the setting of a few basic parameters, such as the number of grey wolves and the maximum number of iterations, and it does not have a complex mathematical model, thus reducing the computation time. (b) High convergence speed: Since the GWOA is inspired by the social behavior of grey wolves, it can converge to the best solution quickly, and the leader of the grey wolf pack guides other grey wolves to search over time and further modify the speed of the solution, thus increasing the search speed. (c) Global search capability: The GWOA does not limit itself to the search of local optimal values; by comparing the adaptation values and location information of the top three and other solutions, the GWOA can perform a global search and find the optimal solution. Therefore, the method can utilize the position and behavior of the leading grey wolf to guide other solutions to update results, which helps the algorithm to quickly converge to the best solution and thus find the best global value.

3.1 Conventional GWOA

The steps in a conventional GWOA search are as follows:

Step 1: The number of grey wolves, ω_T; the maximum iteration number *Max_t*; the initial GWOA parameters *A*, *C*, *a*; and the fitness values are set for each grey wolf.

Step 2: The locations of the top three grey wolves are set in terms of the fitness value as X_α, X_β, and X_δ, where the grey wolf at X_α with the best fitness value is marked as the current optimum.

Step 3: Apply Eq. (1) to calculate the distances between the location values $X_\omega(t)$ of the other grey wolves ω (i.e., not the top three) and those (X_α, X_β, X_δ) of the top three grey wolves. The location value (i.e., fitness value) of each grey wolf ω is then renewed using Eqs. (2) and (3).

$$\begin{cases} D_\alpha(t) = \left| C \cdot X_\alpha(t) - X_\omega(t) \right| \\ D_\beta(t) = \left| C \cdot X_\beta(t) - X_\omega(t) \right| \\ D_\delta(t) = \left| C \cdot X_\delta(t) - X_\omega(t) \right| \end{cases} \tag{1}$$

$$\begin{cases} X_1(t+1) = X_\alpha(t) - A \cdot D_\alpha(t) \\ X_2(t+1) = X_\beta(t) - A \cdot D_\beta(t) \\ X_3(t+1) = X_\delta(t) - A \cdot D_\delta(t) \end{cases} \tag{2}$$

$$X_\omega(t+1) = \frac{[X_1(t+1) + X_2(t+1) + X_3(t+1)]}{3} \tag{3}$$

Here, *A* and *C* are the iteration parameters; $D_\alpha(t)$, $D_\beta(t)$, and $D_\delta(t)$ are the distances between the random location values of the top three grey wolves α, β, δ and the location values of the other grey wolves ω (i.e., not the top three); $X_\omega(t)$ is the current location value of grey wolf ω; $X_1(t+1)$, $X_2(t+1)$, and $X_3(t+1)$ are the location values of the other grey wolves ω (i.e., not the top three) after renewal in accordance with the location values of the top three grey wolves; and $X_\omega(t+1)$ is the mean location value (i.e., the new fitness value) of each grey wolf ω after renewal.

Step 4: Renew parameters *A*, *C*, and *a* as

$$A = 2a \cdot r_1 - a, \tag{4}$$

$$C = 2 \cdot r_2, \tag{5}$$

where *a* is linearly reduced from 2 to 0 by increasing the number of iterations, and r_1 and r_2 are random numbers in the interval [0, 1].

Step 5: If the number of iterations reaches *Max_t*, the iteration stops. The top three fitness values X_α, X_β, and X_δ are then recorded together with the output optimal fitness value X_α. When compliance with the conditions is not achieved, the process returns to Step 2.

3.2 Improved GWOA

The GWOA has advantages of simplicity, high search speed, highly precise searching, and ease of use, making it a valuable and extremely useful algorithm. However, at the time of its inception, the GWOA was a new type of biological intelligence optimization algorithm and the studies were still at an early stage, and the theory and development of this algorithm are still incomplete. In Ref. 23, an improved GWOA with higher performance was proposed. It focuses on the parameter a of the conventional GWOA, adjusting it using Eq. (6), which allows the GWOA to search for the optimum with a larger step in the initial iteration.

$$\Delta a = a_o - \left[a_o \times \left(\frac{t}{Max\_t} \right)^2 \right] \tag{6}$$

Max_t: the maximum number of iterations (set to 50), t: the current number of iterations, a_o: the initial iteration parameter (set to 2), ω_T: the number of grey wolves (set to 5).

Consequently, the iteration parameter a is finely tuned as outlined in Table 2 so that the parameters change with the slope of the P–V characteristic curve. This accelerates the escape from local optima and allows a faster acquisition of the global optimum. The iteration parameters a in Table 2 are only adjusted when $\Delta P > 0$, since this inequality indicates that the current adjustment of parameter a increases the output power of the PVMA, meaning that the next adjustment of a will accelerate tracking towards the MPP. Figure 3 shows the variation in a with

Table 2
Adjustment of parameters according to the slope of the P–V characteristic curve for the improved GWOA.[23]

Item	Condition	
	$m \triangleq \frac{P(t+1)-P(t)}{V(t+1)-V(t)}$	$\Delta P = P(t+1) - P(t)$ $\Delta P > 0$
1	$m > 2$	$a = \Delta a + 0.05$
2	$2 \geq m > 1.5$	$a = \Delta a + 0.03$
3	$1.5 \geq m > 1$	$a = \Delta a - 0.01$
4	$1 \geq m > 0.5$	$a = \Delta a - 0.03$
5	$0.5 \geq m > 0$	$a = \Delta a - 0.05$
6	$m = 0$	$a = \Delta a$
7	$0 > m \geq -0.5$	$a = \Delta a - 0.05$
8	$-0.5 > m \geq -1$	$a = \Delta a - 0.03$
9	$-1 > m \geq -1.5$	$a = \Delta a - 0.01$
10	$-1.5 > m \geq -2$	$a = \Delta a + 0.03$
11	$m < -2$	$a = \Delta a + 0.05$

the number of iterations and the slope of the *P–V* characteristic curve, Fig. 4 shows the relationship between the slope *m* of the *P–V* characteristic curve of the PVMA and the variation in array output power Δ*P*, and Fig. 5 shows the iteration flow chart for the improved GWOA. However, this improved GWOA is only limited to the simulation stage, and its robustness has not yet been verified owing to the limited number of test cases. In response to this shortcoming, the improved GWOA proposed in this paper is evaluated in more practical test cases, and 0.8 times the MPPT voltage under STC was set as the starting voltage to conduct GMPP tracking and verify its robustness.

4. Adopted High-step-up Soft-switching Converter

Figure 6 shows the circuit architecture of the adopted high-step-up soft-switching converter.[21] In the circuit, the energy storage inductor of a conventional boost converter was replaced with a coupled inductor. This allowed the voltage conversion ratio to be increased by the turn ratio of the coupled inductor.[24] Moreover, a resonant branch was connected in the converter to achieve the zero-voltage switching (ZVS) function of the main switch initiated by a

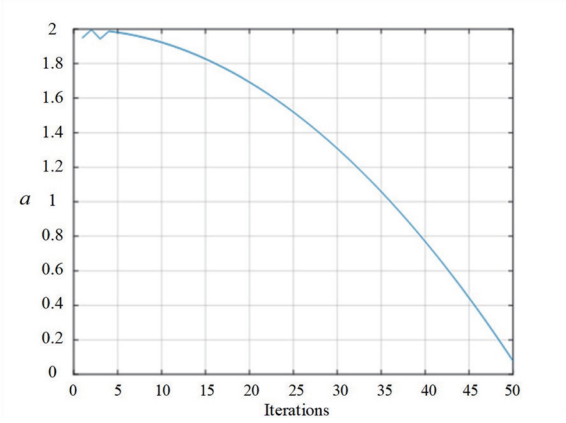

Fig. 3. (Color online) Variation in a with the number of iterations for the improved GWOA.[23]

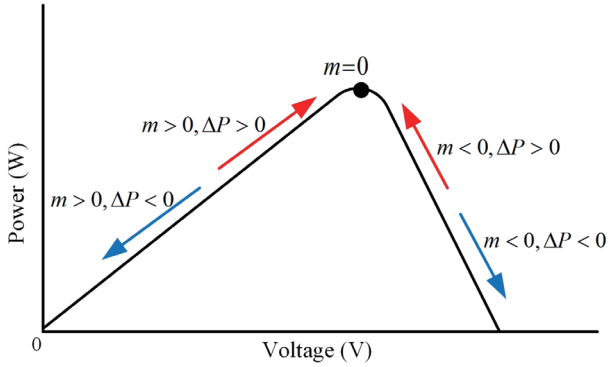

Fig. 4. (Color online) Relationship between the slope *m* of the *P–V* characteristic curve and the PVMA output power variation.[23]

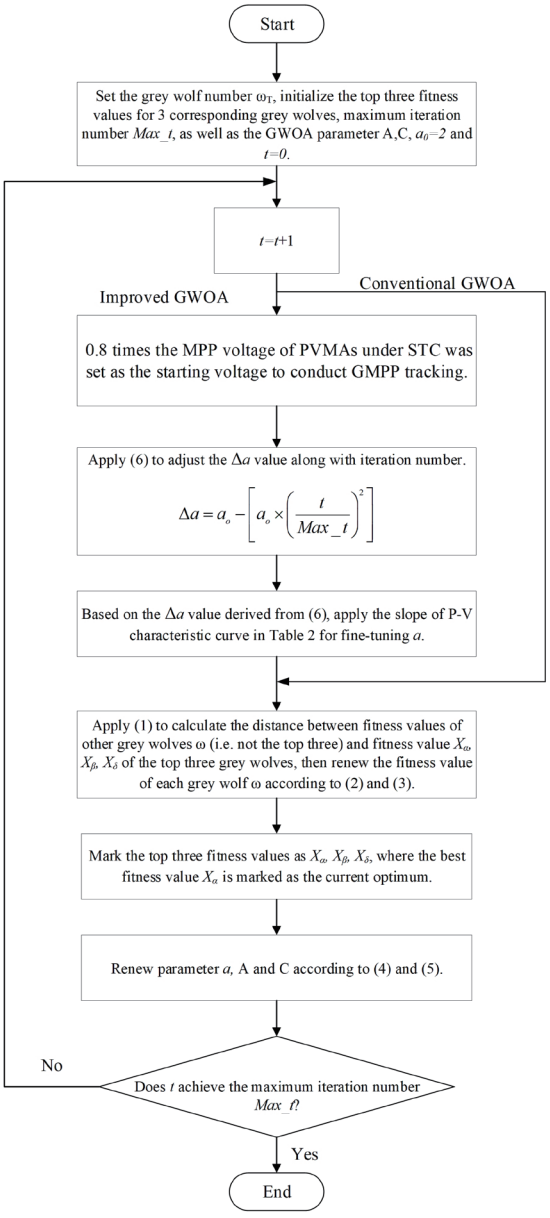

Fig. 5. Iteration flow chart of the improved GWOA.

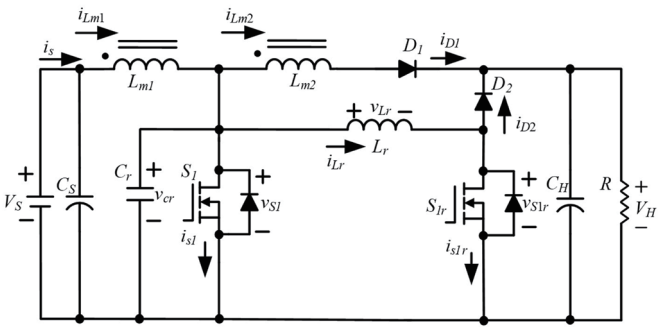

Fig. 6. Circuit architecture of the adopted high-step-up soft-switching converter.[21]

switch control signal. This converter has advantages of a simple circuit architecture and ease of control.[25,26] The relevant electrical specifications of the high-step-up soft-switching converter[21] are given in Table 3. Table 4 shows the circuit component values and parameters.[21]

5. Experimental Results

A TMS320F2809 digital signal processor (DSP) from Texas Instruments was rebuilt to realize the adopted high-step-up soft-switching converter and the MPPT controller used in this study. Figures 7 and 8 present the voltage and current sensor circuits for the MPPT of the PVMA, respectively. The appearance of the overall hardware circuitry is shown in Fig. 9 and the experimental test bench used in this study is shown in Fig. 10.

5.1 Test results of MPPT for improved GWOA

The Chroma ATE 62050H-600S programmable DC power supply[27] offers the function of simulating the output characteristics of PVMAs. It can simulate the actual *P–V* and *I–V* output

Table 3
Electrical specifications of the high-step-up soft-switching converter.[21]

DC input voltage on low-voltage side, V_S	V_S = 70 V ± 10%
DC output voltage on high-voltage side, V_H	V_H = 400 V
Switching frequency, f	f = 25 kHz
Turn ratio of coupled inductor, N	$N = \frac{N_2}{N_1} = 2$
Rated output power, P	P = 300 W

Table 4
Parameters of each component of the high-step-up soft-switching converter.[21]

Coupled inductance, L_{m1}	L_{m1} = 872 μH
Resonant inductance, L_r	L_r = 872 μH
Resonant capacitance, C_r	C_r = 140 pF
Capacitance on low-voltage side, C_S	C_S = 220 μF / 400 V
Capacitance on high-voltage side, C_H	C_H = 470 μF / 500 V
Main switch, S_1	MOSFET-TK49N65W (650 V/49 A)
Resonant switch, S_{1r}	MOSFET-TK49N65W (650 V/49 A)

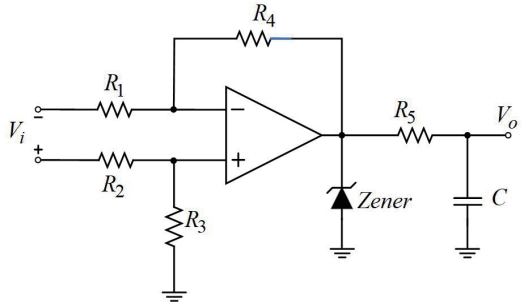

Fig. 7. Voltage-sensing circuit for MPPT of PVMA.

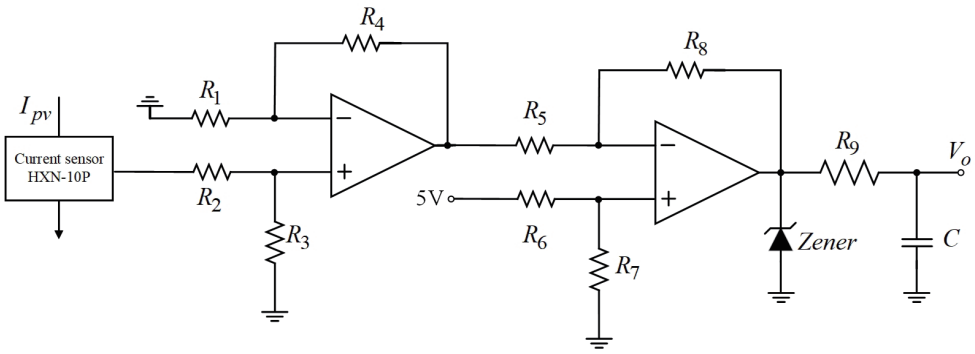

Fig. 8. Current-sensing circuit for MPPT of PVMA.

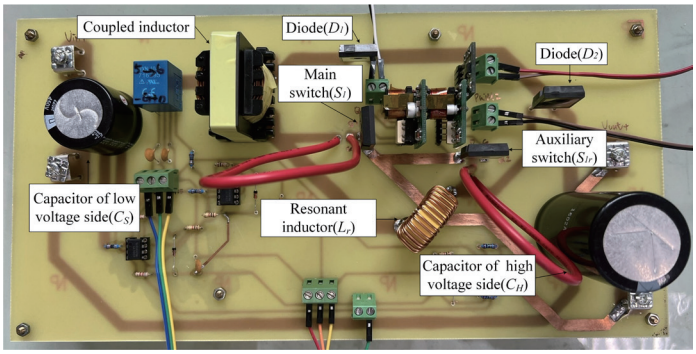

Fig. 9. (Color online) Appearance of physical circuit for high-step-up soft-switching converter.

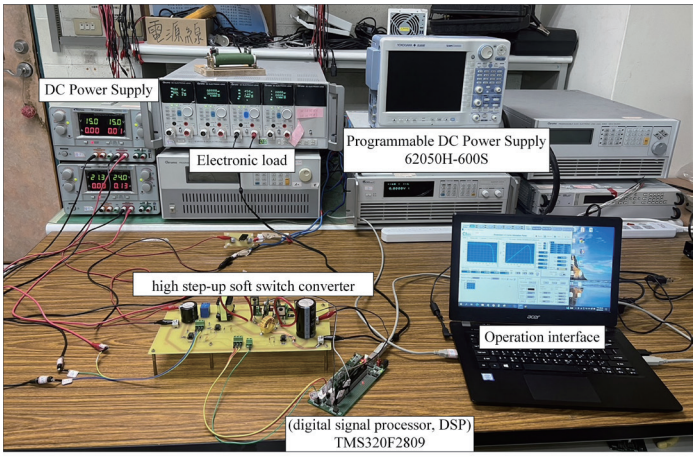

Fig. 10. (Color online) Experimental test bench used with the MPPT controller.

curves of PVMAs under different temperature, sunlight intensity, and shading conditions, and can output and display the MPPT status of PVMAs in real time and record their output waveforms simultaneously.

Therefore, a Chroma ATE 62050H-600S programmable DC power supply[27] was used in our laboratory experiments to mimic the output of a PVMA. Table 5 shows five test cases of different mimicked series–parallel connection configurations with different degrees of shading. Different peak values appeared in the *P–V* curves depending on how many modules were shaded and the shading ratio for each module. Subsequently, actual tests of MPPT were implemented using a conventional GWOA and two other types of improved GWOA. The tracking performance characteristics of these methods were then compared.

Case 1: Four modules in series and three in parallel: (0% shading +0% shading +0% shading +0% shading)//(0% shading +0% shading +0% shading +0% shading)// (0% shading +0% shading +0% shading +0% shading)

Figure 11 shows the *I–V* and *P–V* characteristic curves for Case 1, obtained from an actual test conducted on the PVMA with four modules in series and three in parallel. The normal operation of the PVMA without any shading gave a maximum output power of 244.5 W. Figures 12–14 respectively show the actual MPPT test results with a conventional GWOA, an improved GWOA with only the iteration parameters adjusted, and an improved GWOA with the iteration parameters adjusted and the initial tracking voltage set at 0.8 times the MPP voltage V_{mp} of the PVMA under STCs. The figures show that when one peak appeared in the *P–V* characteristic curve, all three MPPT methods could successfully track the MPP, particularly the improved GWOA with the iteration parameters adjusted and the initial tracking voltage set at $0.8V_{mp}$. In this case, the initial tracking point was closest to the MPP, and the tracking speed and steady-state performance were higher than those of the other methods.

Table 5
Five test cases of different mimicked series–parallel connection configurations with different degrees of shading.

Case	Series–parallel connecting configuration and shading status	Number of peaks in *P–V* curve
1	Four modules in series and three in parallel: (0% shading +0% shading +0% shading +0% shading) //(0% shading +0% shading +0% shading +0% shading) //(0% shading +0% shading +0% shading +0% shading)	1
2	Four modules in series and three in parallel: (0% shading +0% shading +0% shading +90% shading) //(0% shading +0% shading +0% shading +0% shading) //(0% shading +0% shading +0% shading +0% shading)	2 (peak value at left)
3	Four modules in series and three in parallel: (0% shading +0% shading +70% shading +90% shading) //(0% shading +0% shading +70% shading +90% shading) //(0% shading +0% shading +0% shading +0% shading)	3 (peak value at left)
4	Four modules in series and three in parallel: (0% shading +20% shading +40% shading +90% shading) //(0% shading +0% shading +0% shading +0% shading) //(0% shading +0% shading +0% shading +0% shading)	4 (peak value second from right)
5	Four modules in series and three in parallel: (0% shading +70% shading +80% shading +90% shading) //(0% shading +70% shading +80% shading +90% shading) //(0% shading +70% shading +80% shading +90% shading)	4 (peak value at left end)

+ : series; // : parallel.

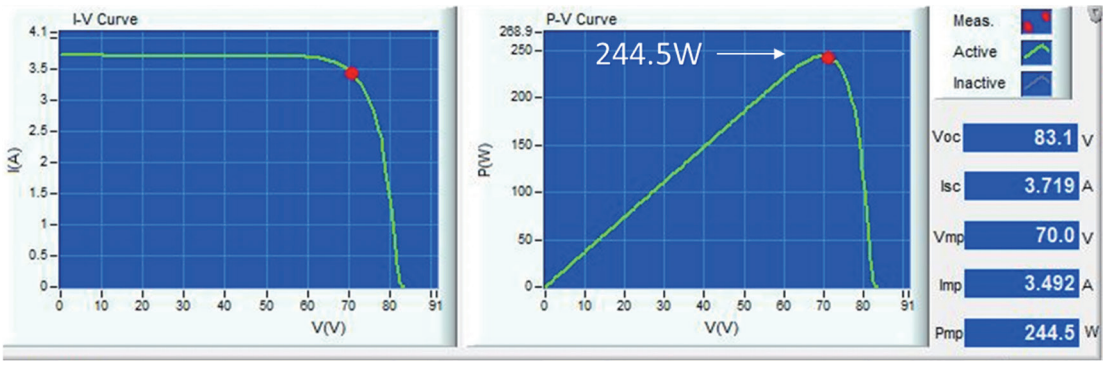

Fig. 11. (Color online) Characteristic *I–V* and *P–V* curves of actual test in Case 1.

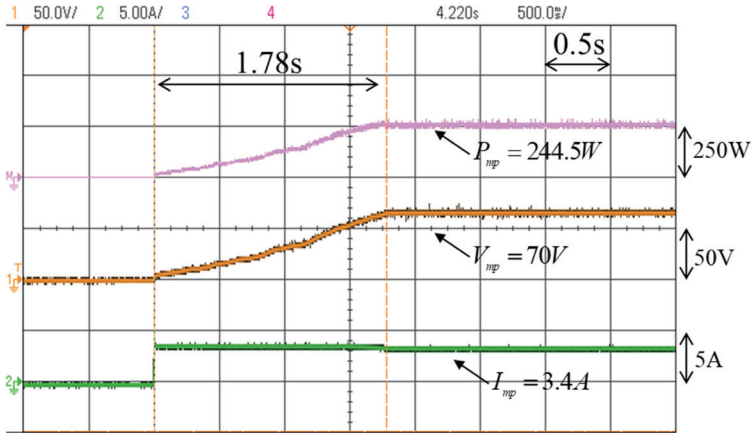

Fig. 12. (Color online) Actual test results for MPPT of conventional GWOA in Case 1.

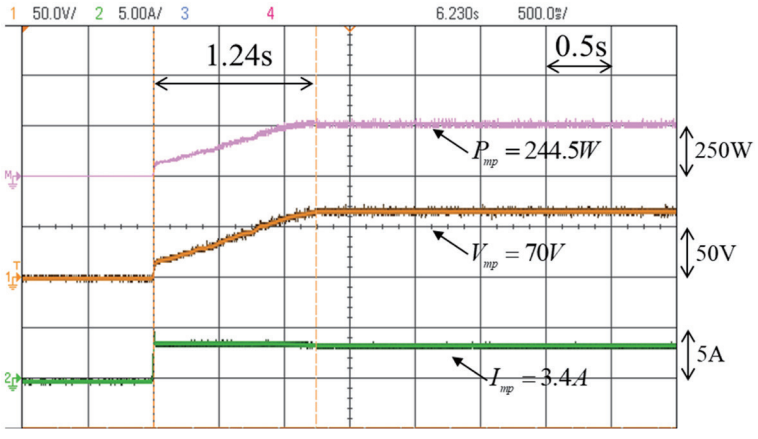

Fig. 13. (Color online) Actual test results for MPPT of improved GWOA in Case 1 with iteration parameters adjusted.

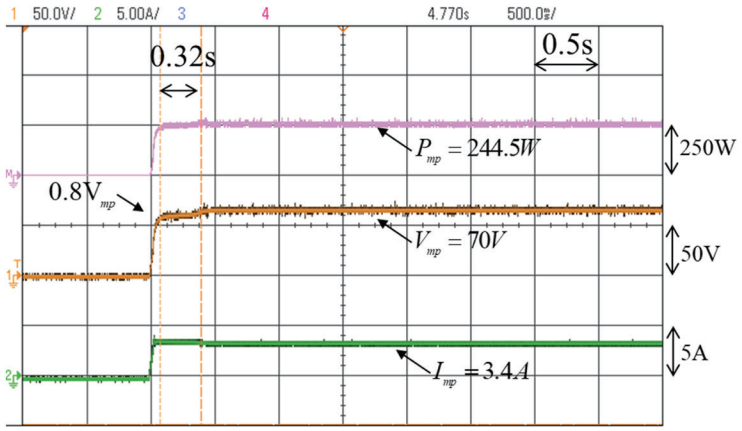

Fig. 14. (Color online) Actual test results for MPPT of improved GWOA in Case 1 with iteration parameters adjusted and initial tracking voltage set at 0.8V_{mp}.

Case 2: Four modules in series and three in parallel: (0% shading +0% shading +0% shading +90% shading)//(0% shading +0% shading +0% shading +0% shading)// (0% shading +0% shading +0% shading +0% shading)

Figure 15 shows the *I–V* and *P–V* characteristic curves for Case 2, obtained from an actual test conducted on the PVMA. Because one module in the array was 90% shaded, two peaks appeared in the *P–V* characteristic curve and the true MPP was on the left at a value of 195.3 W. Figures 16–18 respectively show the actual test results of MPPT for the conventional GWOA, the improved GWOA with only the iteration parameters adjusted, and the improved GWOA with the iteration parameters adjusted and the initial tracking voltage set at 0.8V_{mp}. The figures show that when two peaks appeared in the *P–V* characteristic curve and the true MPP was near 0.8V_{mp}, the tracking response of the improved GWOA with the iteration parameters adjusted and the initial tracking voltage set at 0.8V_{mp} was 1.75 s faster than that of the conventional GWOA and 1.23 s faster than that of the GWOA with only the iteration parameters adjusted.

Case 3: Four modules in series and three in parallel: (0% shading +0% shading +70% shading +90% shading)//(0% shading +0% shading +70% shading +90% shading)// (0% shading +0% shading +0% shading +0% shading)

Figure 19 shows the *I–V* and *P–V* characteristic curves for Case 3, obtained from testing the PVMA. Two modules in the array were 70 and 90% shaded, and three peaks appeared in the *P–V* characteristic curve. The true MPP was on the left at a value of 124.9 W. Figures 20–22 respectively show the actual MPPT test results for the conventional GWOA, the improved GWOA with only the iteration parameters adjusted, and the improved GWOA with the iteration parameters adjusted and the initial tracking voltage set at 0.8V_{mp}. The figures show that when three peaks appeared in the *P–V* characteristic curve, although all three methods could track the true MPP, the tracking speed was highest for the improved GWOA with the iteration parameters adjusted and the initial tracking voltage set at 0.8V_{mp}.

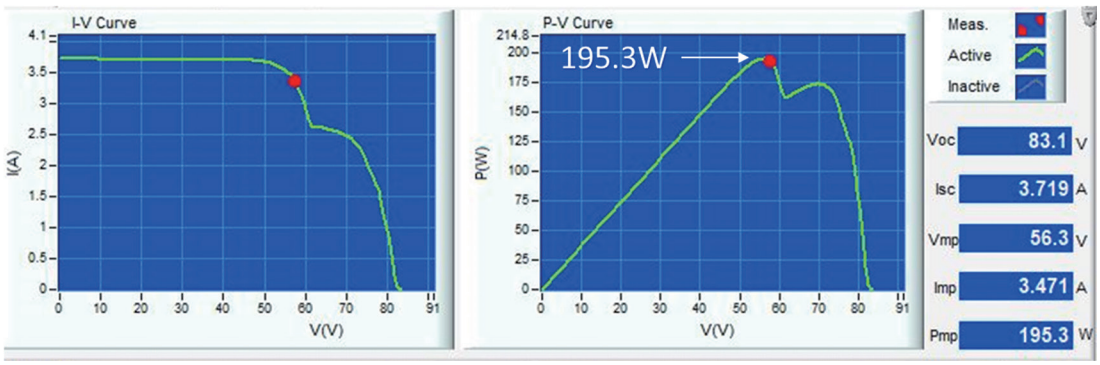

Fig. 15. (Color online) Characteristic *I*–*V* and *P*–*V* curves of actual test in Case 2.

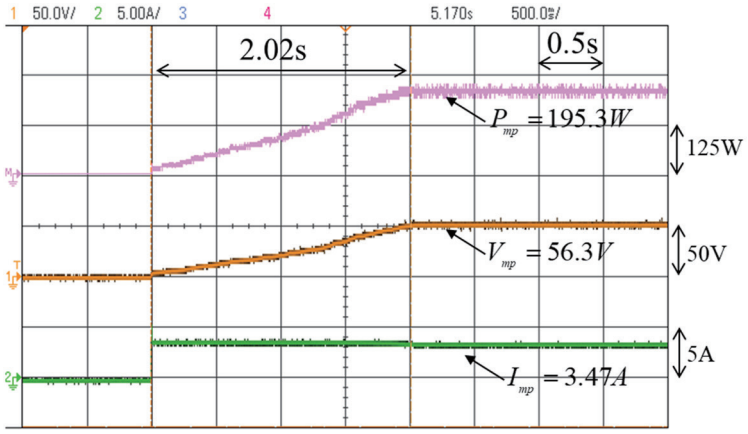

Fig. 16. (Color online) Actual test results for MPPT of conventional GWOA in Case 2.

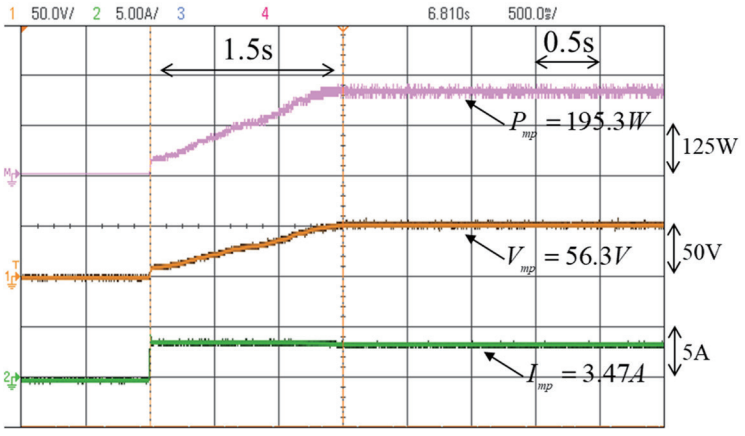

Fig. 17. (Color online) Actual test results for MPPT of improved GWOA in Case 2 with only iteration parameters adjusted.

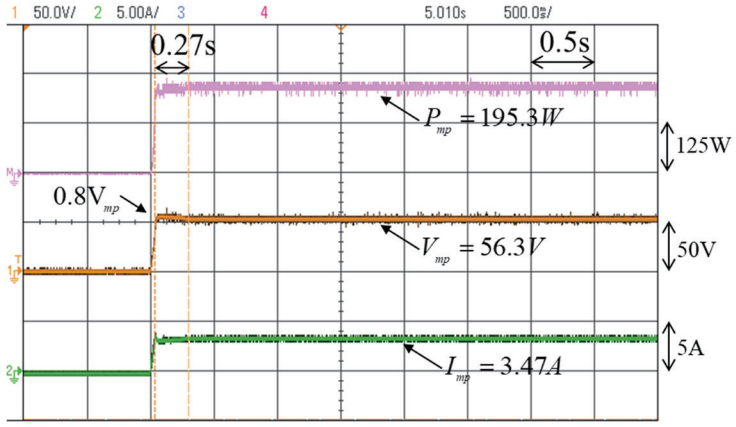

Fig. 18. (Color online) Actual test results for MPPT of improved GWOA in Case 2 with iteration parameters adjusted and initial tracking voltage set at $0.8V_{mp}$.

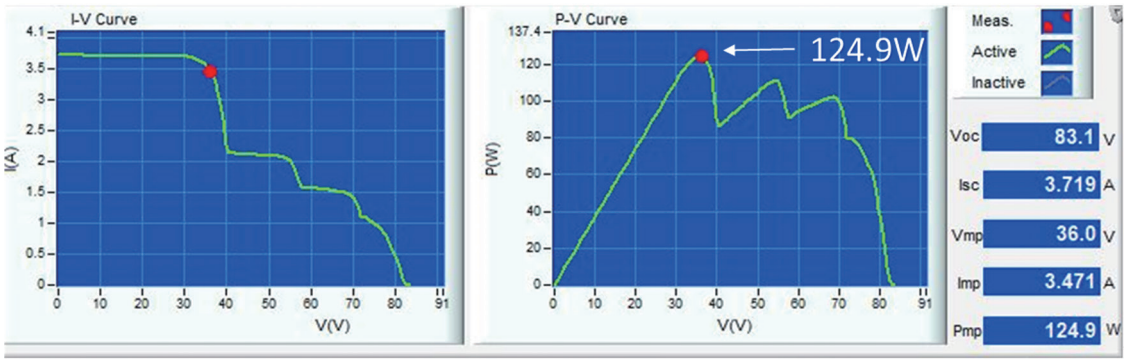

Fig. 19. (Color online) Characteristic *I–V* and *P–V* curves of actual test in Case 3.

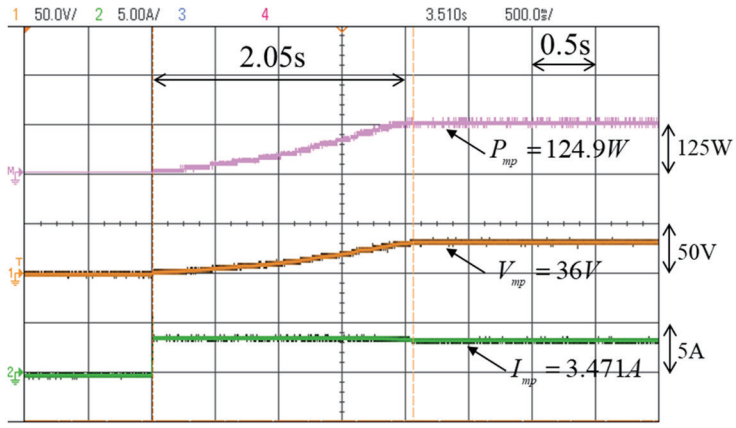

Fig. 20. (Color online) Actual test results for MPPT of conventional GWOA in Case 3.

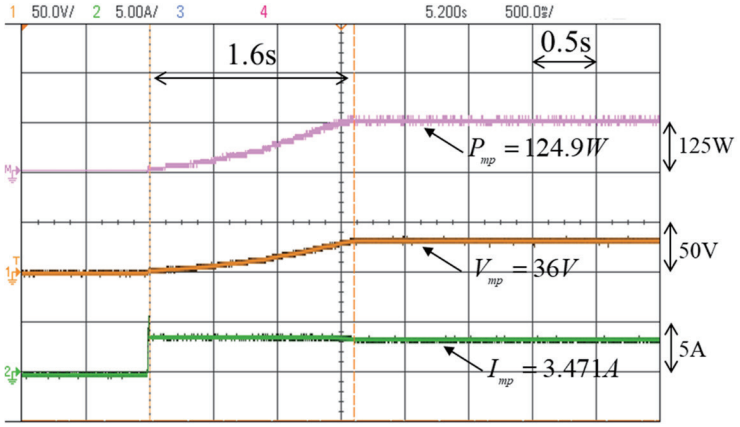

Fig. 21. (Color online) Actual test results for MPPT of improved GWOA in Case 3 with iteration parameters adjusted.

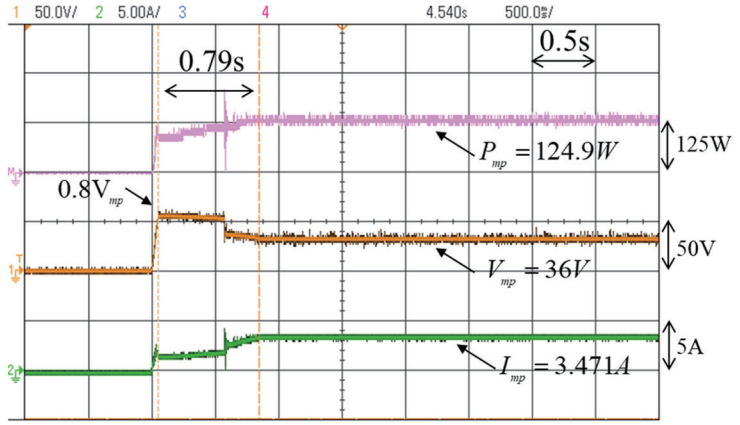

Fig. 22. (Color online) Actual test results for MPPT of improved GWOA in Case 3 with iteration parameters adjusted and initial tracking voltage set at 0.8V_{mp}.

Case 4: Four modules in series and three in parallel: (0% shading +20% shading +40% shading +90% shading)//(0% shading +0% shading +0% shading +0% shading)// (0% shading +0% shading +0% shading +0% shading)

Figure 23 shows the *I–V* and *P–V* characteristic curves for Case 4. Because three modules in the array were 20, 40, and 90% shaded, four peaks appeared in the *P–V* characteristic curve and the true MPP value of 175.3 W was on the third peak. Figures 24–26 respectively show the actual MPPT test results for the conventional GWOA, the improved GWOA with only the iteration parameters adjusted, and the improved GWOA with the iteration parameters adjusted and the initial tracking voltage set at 0.8V_{mp}. The figures show that when four peaks appeared in the *P–V* characteristic curve, although both the conventional GWOA and the improved GWOA with only

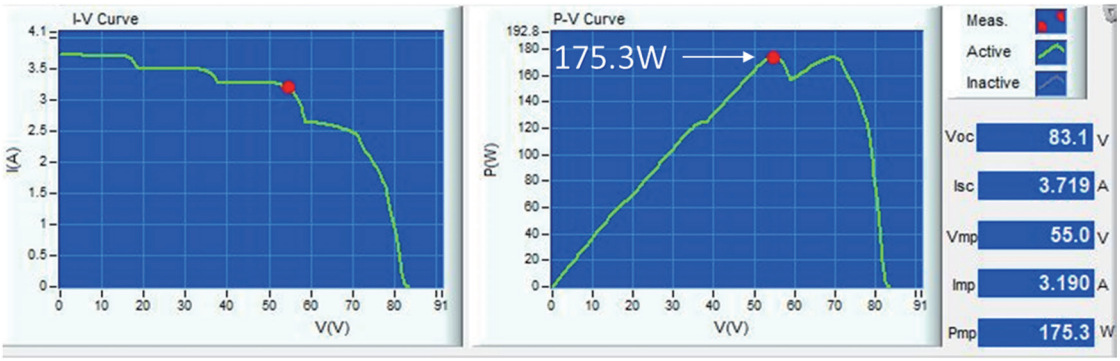

Fig. 23. (Color online) Characteristic I–V and P–V curves of actual test in Case 4.

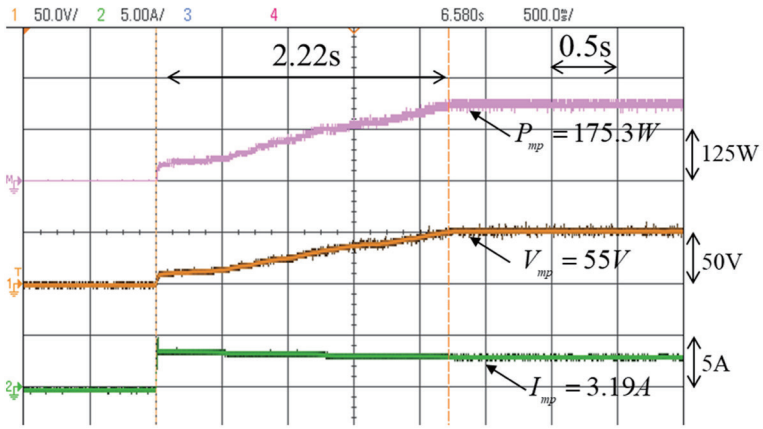

Fig. 24. (Color online) Actual test results for MPPT of conventional GWOA in Case 4.

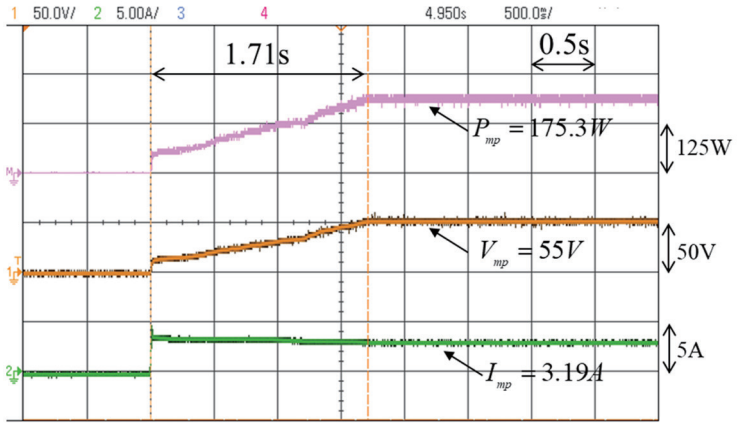

Fig. 25. (Color online) Actual test results for MPPT of improved GWOA in Case 4 with only iteration parameters adjusted.

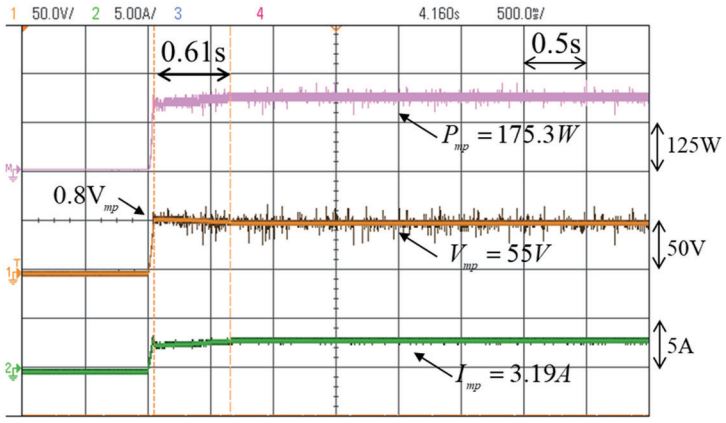

Fig. 26. (Color online) Actual test results for MPPT of improved GWOA in Case 4 with iteration parameters adjusted and initial tracking voltage set at $0.8V_{mp}$.

the iteration parameters adjusted could track the true MPP, the tracking speed was low. When the iteration parameters were adjusted and the initial tracking voltage was set at $0.8V_{mp}$, the improved GWOA could easily escape an LMPP and the true MPP was quickly tracked.

Case 5: Four modules in series and three modules in parallel: (0% shading +70% shading +80% shading +90% shading)//(0% shading +70% shading +80% shading +90% shading)//(0% shading +70% shading +80% shading +90% shading)

Figure 27 shows the *I–V* and *P–V* characteristic curves obtained by testing for Case 5. Because three modules in the array were 70, 80, and 90% shaded, four peaks appeared in the *P–V* characteristic curve and the true MPP was on the left end at a value of 61.12 W. Figures 28–30 respectively display the actual MPPT test results for the conventional GWOA, the improved GWOA with only the iteration parameters adjusted, and the improved GWOA with the iteration parameters adjusted and the initial tracking voltage set at $0.8V_{mp}$. The figures show that when four peaks appeared in the *P–V* characteristic curve, the conventional GWOA and the improved GWOA with only the iteration parameters adjusted easily fell into an LMPP, resulting in a low tracking speed. However, when the iteration parameters were adjusted and the initial tracking voltage was set at $0.8V_{mp}$, the GWOA tracking speed was high.

5.2 Comparison between actual test results of each case

In this study, a conventional GWOA, an improved GWOA with only the iteration parameters adjusted, and an improved GWOA with the iteration parameters adjusted and the initial tracking voltage set at $0.8V_{mp}$ were used. Twenty actual MPPT tests were conducted for the five cases, where the average times from the start of tracking to the true MPP were calculated and compiled, as given in Table 6. The table shows that for all 20 tests of the improved GWOA for all five cases, the average tracking times were shorter than those obtained with the conventional GWOA. The

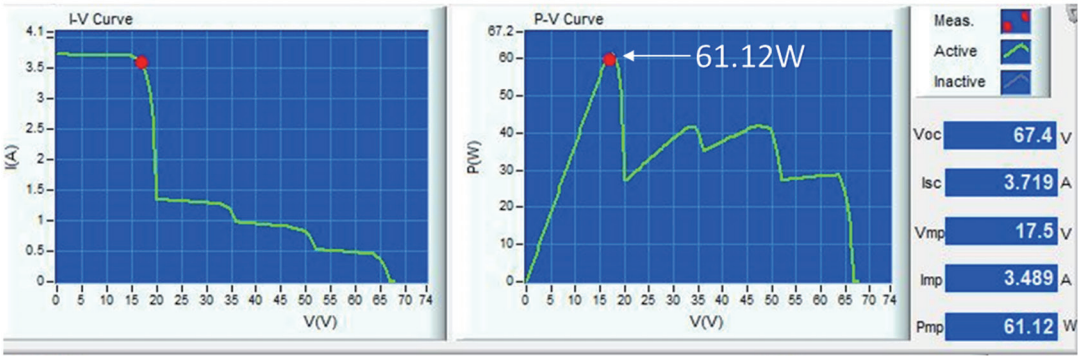

Fig. 27. (Color online) Characteristic I–V and P–V curves of actual test in Case 5.

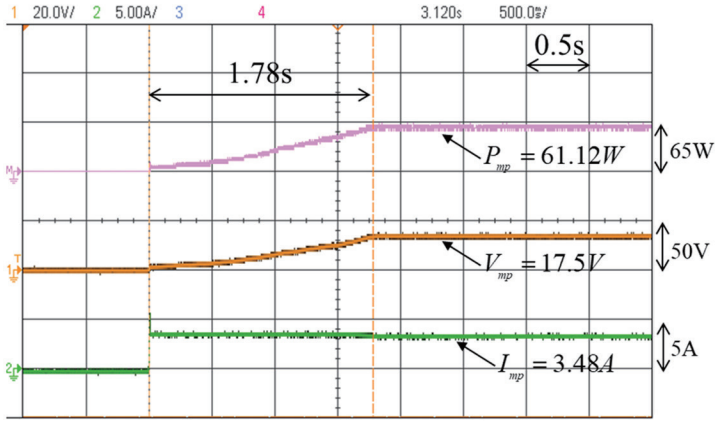

Fig. 28. (Color online) Actual test results for MPPT of conventional GWOA in Case 5.

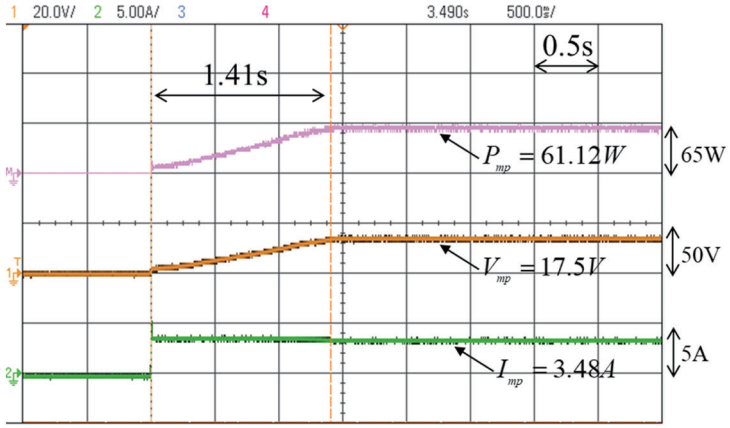

Fig. 29. (Color online) Actual test results for MPPT of improved GWOA in Case 5 with only iteration parameters adjusted.

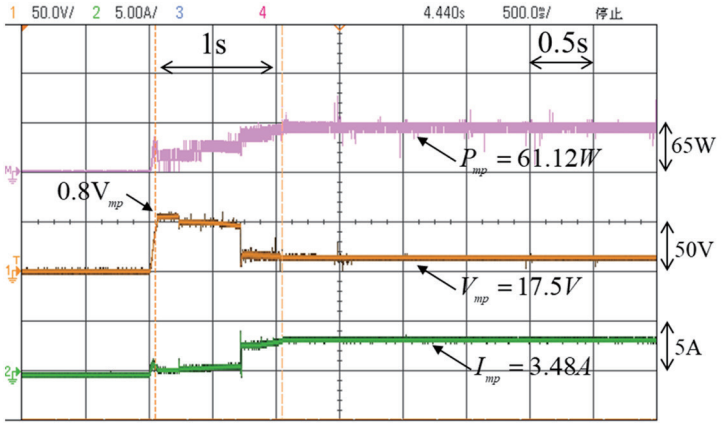

Fig. 30. (Color online) Actual test results for MPPT of improved GWOA in Case 5 with iteration parameters adjusted and initial tracking voltage set at $0.8V_{mp}$.

Table 6
Test results for five different series–parallel connection configuration and shading conditions.

Case	Number of peaks in P–V curve	Average tracking time (s) (% reduction of tracking time compared with conventional GWOA)		
		Conventional GWOA	Improved GWOA with only iteration parameters adjusted	Improved GWOA with iteration parameters adjusted and initial tracking voltage set at $0.8V_{mp}$
1	1	2.3	1.2 (47.8%)	0.5 (78.3%)
2	2 (peak value on left)	2.4	1.0 (58.3%)	0.7 (70.8%)
3	3 (peak value at left)	3.5	2.4 (31.4%)	1.5 (57.1%)
4	4 (peak value second from right)	4.3	3.5 (18.6%)	1.8 (58.1%)
5	4 (peak value at left end)	4.2	3.4 (19.0%)	2.8 (33.3%)

improved GWOA with the iteration parameters adjusted and the initial tracking voltage set at $0.8V_{mp}$ gave the highest tracking performance. For the different numbers of peaks in the P–V characteristic curves, the average tracking time of the improved GWOA with only the iteration parameters adjusted was reduced by 19.0–58.3% compared with that of the conventional GWOA. However, the average tracking time of the improved GWOA with both the iteration parameters adjusted and the initial tracking voltage set at $0.8V_{mp}$ was 33.3–78.3% shorter than that of the conventional GWOA.

5.3 Discussion

The main contribution of this paper is to improve the tracking speed and efficiency of the GWOA for MPPT by improving the conventional GWOA so that the step size factor in the iteration formula can be automatically adjusted online according to the number of iterations and the slope of the *P–V* characteristic curve of the PVMA. This allows the PVMA to jump out of an LMPP when the *P–V* characteristic curve has multiple peaks due to the shading of some modules and to track the GMPP accurately and quickly. In addition, to further enhance the speed response of the MPPT, the starting tracking voltage was set to 0.8 times the MPP voltage of the PVMA under STC. The GMPP tracking performance was evaluated for five cases with different numbers of peaks in the *P–V* characteristics and different locations of the GMPP under different shading conditions, as shown in Table 6, and the proposed improved GWOA GMPP method was verified to provide higher performance than the conventional GWOA. In this paper, we proposed an improved GWOA applicable to a PVMA for MPPT and used the developed high-step-up soft-switching converter for MPPT, with a TMS320F2809 DSP from Texas Instruments used as the control core. Using the iteration formula of the proposed improved GWOA, the most appropriate duty cycle is found, then the final grey wolf position value is used as the optimal target function value to realize MPPT control. An MPPT test was conducted under five different shading conditions of the PVMA as shown in Table 5. The MPPT test result of the proposed improved GWOA was compared with the tracking response of the conventional GWOA and the time to reach the GMPP as a basis for performance comparison. The test results are shown in Table 6. In addition, to further verify that the tracking performance is superior to those of the other existing smart algorithms,[6,8,12] the average tracking times of 20 MPPT tests under four different shading conditions, resulting in different numbers of peaks in the *P–V* characteristic curves and different locations of the GMPP of the PVMA, are shown in Table 7 for comparison. From Table 7, it can be observed that the proposed MPPT with the simultaneous adjustment of the iteration parameters and the improved GWOA with an initial tracking voltage of $0.8V_{mp}$ has a faster tracking response than the other smart MPPT methods.[6,8,12]

Table 7
Comparison of actual test results for four cases with those using other smart MPPT methods.

Case	Number of peaks of *P–V* curve	Method proposed in Ref. 6	Method proposed in Ref. 8	Method proposed in Ref. 12	Method proposed in this study
		Average tracking time (s)	Average tracking time (s)	Average tracking time (s)	Average tracking time (s)
1	1	0.8	2.5	4.5	0.5
2	2	1.2	4.1	4.3	0.7
3	3	1.9	5.6	5.1	1.5
4	4	None*	None*	6.6	1.8

None*: The reference does not provide the test results for this case.

6. Conclusions

In this study, two improved GWOAs were used for the MPPT of a PVMA. The proposed improved GWOA with adjusted iteration parameters and the initial voltage for tracking set at $0.8V_{mp}$ showed much higher performance. From actual test results, it was shown that the partial shading of some modules of a PVMA resulted in the generation of multiple peaks in the P–V characteristic curve, and the improved GWOA with the iteration parameters adjusted and the initial tracking voltage set at $0.8V_{mp}$ provided a faster tracking speed response than conventional GWOAs and also the improved GWOA with only the iteration parameters adjusted. The proposed improved GWOA can be applied to all systems with multipeak characteristics to identify the optimal value without trapping at a local maximum position, thus increasing the speed of reaching an MPP. When applied to photovoltaic power generation systems for MPPT, the improved algorithm will not only improve the efficiency of power generation, but also adapt to different environmental conditions, enabling photovoltaic power generation systems to be used more effectively and improving their economic efficiency and viability.

Acknowledgments

This work was supported by the National Science and Technology Council, Taiwan, under Grant no. NSTC 112-2221-E-167-002.

References

1 D. Sera, L. Mathe, T. Kerekes, S. V. Spataru, and R. Teodorescu: IEEE J. Photovolt. **3** (2013) 1070. https://doi.org/10.1109/JPHOTOV.2013.2261118
2 J. Ahmed and Z. Salam: IEEE Trans. Sust. Energy **9** (2018) 1487. https://doi.org/10.1109/TSTE.2018.2791968
3 J. Wang, Y. Yi, Y. Yang, G. Zhang, and S. Huang: Proc. 29th Chin. Contr. Decis. Conf. (2017) 2237–2341. https://doi.org/10.1109/CCDC.2017.7978905
4 Y. Ma, X. Zhou, Z. Gao, and T. Bai: Proc. IEEE Intern. Conf. Mechatron. Autom. (2017) 311–315. https://doi.org/10.1109/ICMA.2017.8015834
5 M. Dorigo, M. Birattari, and T. Stutzle: IEEE Comput. Intell. Mag. **1** (2006) 28. https://doi.org/10.1109/MCI.2006.329691
6 G. A. Abdul and M. S. Junita: Proc. 6th UKSim/AMSS Eur. Symp. Comput. Modeling Simulation (2012) 95–100. https://doi.org/10.1109/EMS.2012.65
7 G. C. Catalina, C. Restrepo, S. Kouro, and J. Rodriguez: IEEE Access **9** (2021) 43121. https://doi.org/10.1109/ACCESS.2021.3066281
8 N. Pragallapati, T. Sen, and V. Agarwal: IEEE J. Photovolt. **7** (2017) 624. https://doi.org/10.1109/JPHOTOV.2016.2629844
9 M. Brahmi, C. B. Regaya, H. Hamdi, and A. Zaafouri: Proc. 8th Intern. Conf. Contr. Decis. Inf. Technol. (2022) 1–6. https://doi.org/10.1109/CoDIT55151.2022.9804021
10 P. Megantoro, Y. D. Nugroho, F. Anggara, Suhono, and E. Y. Rusadi: Proc. 2018 3rd Int. Conf. Inf. Technol., Inf. Syst. Electr. Eng. (ICITISEE) (2018) 74–78. https://doi.org/10.1109/ICITISEE.2018.8721031
11 Z. Wu, R. Meng, and R. Cao: Proc. IEEE 5th Conf. Energy Internet Energy Syst. Integration (2021) 22–24. https://doi.org/10.1109/EI252483.2021.9712946
12 R. V. Rao, V. J. Savsani, and D. P. Vakharia: Comput. Aided Des. **43** (2011) 303. https://doi.org/10.1016/j.cad.2010.12.015
13 V. M. Tehrani, A. Rajaei, and M. A. Loghavi: Proc. 12th Power Electron. Drive Syst. Technol. Conf. (2021) 2–4. https://doi.org/10.1109/PEDSTC52094.2021.9405829
14 J. Ahmed and Z. Salam: Proc. 4th Int. Conf. Power Eng., Energy Electr. Drives (2013) 558–562. https://doi.org/10.1109/PowerEng.2013.6635669
15 H. Soneji and R. C. Sanghvi: Proc. World Congr. Inf. Commun. Technol. (2012) 878–883. https://doi.org/10.1109/WICT.2012.6409199

16 K. L. Lian, J. H. Jhang, and I. S. Tian: IEEE J. Photovolt. **4** (2014) 626. https://doi.org/10.1109/JPHOTOV.2013.2297513
17 S. Daraban, D. Petreus, and C. Morel: Proc. 39th IEEE Annual Conf. Ind. Electron. Soc. (2013) 1490–1495. https://doi.org/10.1109/IECON.2013.6699353
18 S. Mirjalili, S. M. Mirjalili, and A. Lewis: Adv. Eng. Softw. **69** (2014) 46. https://doi.org/10.1016/j.advengsoft.2013.12.007
19 R. B. Bollipo, S. Mikkili, and P. K. Bonthagorla: CSEE J. Power and Energy Syst. **7** (2021) 9. https://doi.org/10.17775/CSEEJPES.2019.02720
20 I. S. Millah, P. C. Chang, D. F. Teshome, R. K. Subroto, K. L. Lian, and J. F. Lin: IEEE Open J. Ind. Electron. Soc. **4** (2022) 392. https://doi.org/10.1109/OJIES.2022.3179284
21 K. H. Chao, Y. P. Kuo, and H. H. Chen: IEEE Access **11** (2023) 48506. https://doi.org/10.1109/ACCESS.2023.3276649
22 SunWorld Datasheet: http://www.ecosolarpanel.com/ecosovhu/products/18569387_0_0_1.html.
23 K. H. Huang, K. H. Chao, Y. P. Kuo, and H. H. Chen: Energies **16** (2023) 1. https://doi.org/10.3390/en16114329
24 B. L. Narasimharaju, S. P. Dubey, and S. P. Singh: Proc. 2010 Int. Conf. Ind. Electron., Contr. Robot (2010) 27–29. https://doi.org/10.1109/IECR.2010.5720135
25 K. H. Chao and Y. C. Jheng: Intern. J. Electron. **105** (2017) 164. https://doi.org/10.1080/00207217.2017.1355022
26 K. H. Chao and C. H. Huang: IET Power Electron. **7** (2014) 1557. https://doi.org/10.1049/iet-pel.2013.0335
27 62050H-600S Programmable DC Power Supply, Chroma ATE Inc: https://www.chromaate.com/downloads/catalogue/Power/62000H-TC.pdf.

About the Authors

Kuei-Hsiang Chao received his B.S. degree in electrical engineering from National Taiwan University of Science and Technology, Taipei, Taiwan, in 1988, and his M.S. and Ph.D. degrees in electrical engineering from National Tsing Hua University, Hsinchu, Taiwan, in 1990 and 2000, respectively. He is presently a lifetime distinguished professor at National Chin-Yi University of Technology, Taichung, Taiwan. His areas of interest are computer-based control systems, applications of control theory, renewable energy, and power electronics. Dr. Chao is a life member of the Solar Energy and New Energy Association and a member of the IEEE.

Ying-Piao Kuo received his B.S. degree in electrical engineering in 1985 from National Taiwan University of Science and Technology, Taipei, Taiwan, his M.S. degree in electrical engineering in 1989 from National Taiwan University, and his Ph.D. degree from National Taiwan University of Science and Technology in 2011. In 1989, he joined National Chin-Yi University of Technology, Taichung, Taiwan, where he is currently an associate professor in the Department of Electrical Engineering. His current research interests include the design of switching-mode power supplies, the speed estimation of ac motor drives, partial discharge, and power system stability.

Hong-Han Chen was born in Taipei, Taiwan, in 1999. In 2021, he received a degree in electrical engineering from National Chin-Yi University of Technology, Taichung, Taiwan. He is presently a graduate student in the Electrical Engineering Department of National Chin-Yi University of Technology. His areas of interest are renewable energy, power electronics, and maximum power point tracking for photovoltaic module arrays.